Chemosphere 295 (2022) 133908

Contents lists available at ScienceDirect

Chemosphere

journal homepage: www.elsevier.com/locate/chemosphere

Fixed-bed column study of phosphate adsorption using immobilized phosphate-binding protein

Faten B. Hussein, Brooke K. Mayer *

Department of Civil, Construction and Environmental Engineering, Marquette University, 1637 W Wisconsin Ave, Milwaukee, WI, 53233, USA

HIGHLIGHTS

- PBP-NHS resin provided high P_i selectivity compared to LayneRT™ ion exchange resin.
- PBP-NHS resin's P_i adsorption capacity was not affected by wastewater constituents.
- PBP-NHS resin offered consistent adsorption/desorption over three column cycles.
- Thomas and Yoon-Nelson models had $R^2 > 0.95$ for the column breakthrough data.

GRAPHICAL ABSTRACT

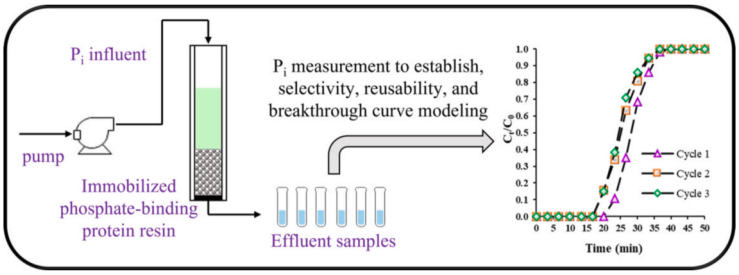

ARTICLE INFO

Handling Editor: Y Yeomin Yoon

Keywords:
Nutrient
PBP
Breakthrough curve
Removal
Recovery
Thomas model

ABSTRACT

Bio-adsorption using high-affinity phosphate-binding proteins (PBP) has demonstrated effective phosphorus removal and recovery in batch-scale tests. Subsequent optimization of design and performance of fixed-bed column systems is essential for scaling up and implementation. Here, continuous-flow fixed-bed column tests were used to investigate the adsorption of inorganic phosphate (orthophosphate, P_i) using phosphate-binding proteins immobilized on resin (PBP–NHS) targeting P_i removal to ultra-low levels followed by recovery. Time to breakthrough decreased with higher influent P_i concentration, smaller bed volume, and higher influent flow rates. The Thomas and Yoon-Nelson breakthrough models adequately described PBP-NHS resin performance with a correlation coefficient of $R^2 > 0.95$. The sharp S-shape of the breakthrough curves for both P_i-only solution and multi-ion solution indicated highly favorable and selective separation of P_i using PBP-NHS resin, beyond that achieved using LayneRT™, a commercial ion exchange resin. The P_i adsorption capacity of the PBP-NHS column was unaffected by competing anions, whereas capacity of the LayneRT™ column dropped by 20%. Tertiary wastewater effluent was also successfully treated in PBP-NHS column tests with a typical S-shaped breakthrough curve. Operating the fixed-bed column in multi-cycle mode evidenced the reusability of PBP-NHS resin with no significant decline in column performance. The results of this study contribute to efforts to scale up designs of PBP-NHS adsorption systems.

* Corresponding author.
E-mail address: brooke.mayer@marquette.edu (B.K. Mayer).

https://doi.org/10.1016/j.chemosphere.2022.133908
Received 5 December 2021; Received in revised form 4 February 2022; Accepted 5 February 2022
Available online 7 February 2022

1. Introduction

Excessive orthophosphate (P_i) released from domestic, agricultural, and industrial activities significantly contributes to eutrophication, which affects water quality and leads to losses in biodiversity. While too much P_i is therefore problematic, conversely, too little P_i also poses major challenges. Mineable phosphate is a finite resource that, on human timescales, is being continuously depleted to supply fertilizers for food production. Therefore, it is vital to efficiently manage P_i usage, and removing and recovering P_i from waste streams whenever viable can contribute to this effort. Numerous technologies have been applied to remove P_i from water/wastewater, including ion exchange resins, chemical precipitation and crystallization, adsorption, membrane technology, and biological treatment (Bui et al., 2018; Huang et al., 2017; Mayer et al., 2013; Xu et al., 2019; S. Yang et al., 2016). Among these technologies, adsorption is a promising approach to remove P_i to low final concentrations (Jia et al., 2020; Mayer et al., 2013; Pap et al., 2020). Advantages include the adsorbents' high selectivity, low cost, and durability in batch or continuous-flow operating modes (Qiu et al., 2017). Adsorption performance, however, depends on the material itself and system conditions such as pH and sorbate concentration (Pap et al., 2020).

Nature offers an effective P_i sorbent in the form of high-affinity phosphate-binding proteins (PBPs) such as PstS, which selectively binds P_i in a deep cleft using 12 hydrogen bonds (Ledvina et al., 1998; Luecke and Quiocho, 1990). Adsorptive systems utilizing PstS have been developed for P_i removal and recovery (Choi et al., 2013; Hussein et al., 2020; Li et al., 2009; Venkiteshwaran et al., 2020, 2018; Y. Yang et al., 2016). Using such systems, effective P_i removal to ultra-low levels, even when starting at low concentrations, has been demonstrated. PBP adsorbents also offer P_i recovery via pH adjustment to desorb the captured molecules in a pure, concentrated form suitable for reuse (Hussein et al., 2020; Venkiteshwaran et al., 2020). PBP features rapid adsorption in comparison to metal oxide adsorbents (Venkiteshwaran et al., 2020). For example, P_i sorption using PBP was 30–240 times faster with 15–100 times higher adsorption affinity compared to zirconium and copper oxides. Moreover, PBP can selectively adsorb P_i even in the presence of the structurally similar arsenate ion (Venkiteshwaran et al., 2021). Previous PBP research predominantly focused on proof-of-concept tests performed in batch systems rather than the more realistic flow-through columns needed to optimize performance for practical application.

Continuous-flow, fixed-bed columns are most practical for wastewater treatment as they efficiently treat large volumetric flowrates (Hu et al., 2020). Fixed-bed column experiments provide reliable information pertaining to breakthrough times, adsorption conditions, and adsorbents' stability during continuous use (Satya et al., 2021; Yanyan et al., 2018). This study examined P_i adsorption using PBP immobilized on a resin material (PBP–NHS) operated in continuous-flow, fixed-bed column mode. The research objectives were to (i) investigate the effect of column operating parameters (influent concentration, bed volume, and flow rate) to establish a basis for large-scale column design; (ii) Evaluate the column's reusability in multi-cycle operating mode and examine its selectivity compared to a commercially available ion exchange resin, LayneRT™; (iii) assess PBP-NHS resin performance treating tertiary wastewater effluent; and (iv) Explore the breakthrough characteristics of the fixed-bed column using the Thomas, Adams-Bohart, Yoon-Nelson, and bed depth service time (BDST) mathematical models.

2. Materials and methods

2.1. Preparation of PBP-NHS resin

The packed-bed material was prepared by immobilizing a purified solution of PBP onto NHS-activated Sepharose resin (schematic illustration is shown in the supplementary data, Fig. S1). This consisted of two major steps, expression and purification followed by immobilization, as described below.

2.1.1. PBP expression and purification

The backbone overexpression plasmid pET22b including the pstS gene (A197C) was obtained from Addgene, USA (plasmid #78198). The plasmid was transformed into *E. coli* BL21(DE3) competent cells, as described by Solscheid et al. (2015). To express and purify PBP, recombinant cells were cultivated in Luria Broth (LB) with 100 mg mL^{-1} ampicillin at 37 °C and vigorous agitation at 250 rpm. Once the cell suspension reached an OD_{600} value of 0.6–0.8, 1 mM isopropyl β-d-1-thiogalactopyranoside (IPTG) was added. The IPTG was allowed to react with the culture for 3–4 h, after which the induced cells were centrifuged for 20 min at 1250×*g*. PBP expression in the cells was confirmed using sodium dodecyl sulfate polyacrylamide gel electrophoresis (SDS-PAGE), as described by Hussein et al. (2020).

To obtain purified PBP solution, the PBP-expressed cell pellet was resuspended in 100 mL of binding buffer (50 mM NaH_2PO_4, 0.5 M NaCl, pH 8.0) and sonicated using a Q500 Sonicator (Qsonica, USA) set at amplitude = 45%, pulse rate = 15 s on and 45 s off. The lysate supernatant was collected following centrifugation at 6700×*g* for 45 min. The supernatant was then added to a Ni Sepharose™ 6 Fast Flow resin column (GE Healthcare Life Sciences, USA) to bind for 60 min at room temperature with gentle agitation. Elution buffer (50 mM NaH_2PO_4, 0.5 M NaCl, 250 mM imidazole, pH 8.0) was used to release the PBP, and 5 mL eluted fractions were collected. The protein's presence was verified in the eluted fractions using SDS-PAGE. The eluted PBP fraction was dialyzed in buffer (0.2 M $NaHCO_3$, 0.5 M NaCl, pH 7), and the PBP concentration was measured using a Pierce™ BCA protein assay kit (Thermo Fisher Scientific, USA). The PBP was stored in 14% glycerol solution at −80 °C until use.

2.1.2. PBP immobilization on NHS-activated Sepharose

To immobilize PBP on the surface of NHS-activated Sepharose, purified PBP samples were dialyzed using a Spectra/Por® 2 dialysis membrane (MWCO 12–14 kDa, Spectrum Laboratories, Inc., USA) to remove the glycerol preservative. PBP dialysis was conducted at room temperature for 2 h with 4–6 exchanges of buffer (0.2 M $NaHCO_3$, 0.5 M NaCl, pH 8). The dialyzed PBP was immobilized on NHS-activated Sepharose™ 4 Fast Flow resins (GE Healthcare Life Sciences, USA) following the manufacturer's instructions (71–5000–14 AD). Briefly, NHS-activated Sepharose resin was washed with 10–15 bed volumes of 1 mM HCl solution at 4 °C. The washed resin was mixed with PBP solution at a 1:1 volumetric ratio. The coupling reaction was performed at room temperature for 4 h.

After reaction completion, the supernatant was collected and the concentration of unbound PBP was measured using a Pierce™ BCA protein assay kit. The binding efficiency of the NHS-activated Sepharose was 60–80%. The modified resin was blocked against non-reacted groups using 2 bed volumes of 0.1 M Tris-HCl at pH 8.5 for 45 min. The resin was then washed with low pH (0.1 M acetate, 0.5 M NaCl, pH 4–5) and high pH (0.1 M Tris-HCl, pH 8–9) buffers in 3 repetitions of alternating wash cycles. To remove the legacy P_i adsorbed on the PBP during the expression and purification process, PBP-NHS resin was washed with 5 bed volumes of Tris buffer at pH 12.5, which completely desorbed P_i from the PBP-NHS resin (Venkiteshwaran et al., 2018). The PBP-NHS resin was kept at 4 °C until use within 48 h.

2.2. Fixed-bed adsorption studies

Continuous-flow, fixed-bed column experiments were conducted to evaluate column performance under various operating parameters: influent concentration, bed volume, flow rate, and multi-cycle operating mode. These tests were performed in well-controlled laboratory buffers. The selectivity of PBP-NHS resin was evaluated in comparison to a commercially available resin, LayneRT™. Additionally, a lab-scale

experiment using tertiary wastewater effluent was performed to further assess the performance of PBP-NHS resin in more realistic settings.

2.2.1. The influence of column operating parameters

PBP-NHS resin was packed into Bio-Rad's Poly-Prep® columns (0.8 cm ID x 4 cm H). A peristaltic pump was used to maintain continuous downflow of P_i solution. Experimental conditions are listed in Table 1. Each set of experiments was conducted in duplicate. Effluent fractions (1.0 mL) were collected at room temperature for all experiments at regular time intervals until the bed was exhausted (i.e., the effluent P_i concentration [C_t] equaled the influent P_i concentration [C_0]). The column's breakthrough point was determined as $C_t/C_0 = 10\%$, and the column's point of exhaustion was $C_t/C_0 = 90\%$. Influent and effluent P_i concentrations were measured using the standard ascorbic acid method (APHA, 2005).

PBP-NHS resin must also be reusable such that the P_i binding ability of the system is restored following desorption (Kuroda et al., 2000). Moreover, the recovered P_i from desorption can be utilized for subsequent reuse. To evaluate the system's reusability, consecutive adsorption-desorption cycles were conducted three times with an influent P_i concentration of 1.1 mg PO_4^{3-} L^{-1}, 1.0 mL bed volume of drained PBP-NHS resin, and 0.2 mL min^{-1} flow rate. The desorption cycle was performed using 3 bed volumes of Tris buffer at pH 12.5. A control column experiment with only NHS resin (without PBP) was also performed to ensure no P_i adsorption was associated with NHS-activated Sepharose. The control test showed that the NHS resin by itself did not adsorb P_i, meaning that all adsorptive performance was derived from the PBP's functionality.

2.2.2. PBP-NHS resin's P_i selectivity

To compare the selectivity of PBP-NHS resin to the commercially available P-selective resin LayneRT™ (Layne Christensen Co., The Woodlands, TX), parallel experiments using P_i-only solution and multi-ion solution were conducted. For PBP-NHS resin, the fixed-bed column was operated with 0.35 g PBP-NHS resin, flow rate of 0.2 mL min^{-1}, and 1.5 mg L^{-1} P_i-only solution (spiked as KH_2PO_4). An identical column was operated with a multi-ion solution containing 1.5 mg L^{-1} each of KH_2PO_4, $MgSO_4$, $CaCl_2$, KNO_3, and $NaHCO_3$. Tests using both water matrices were conducted in duplicate. Analogous experiments were conducted using LayneRT™ resin. The fixed-bed column was performed with 0.35 g LayneRT™ resin, flow rate of 0.2 mL min^{-1}, and P_i-only solution of 1.0 g L^{-1}. For multi-ion solution tests, 1.0 g L^{-1} of each (KH_2PO_4, $MgSO_4$, $CaCl_2$, KNO_3, and $NaHCO_3$), flow rate of 0.2 mL min^{-1}, and 0.35 g LayneRT™ resin were used. Both experiments were conducted in duplicate.

A continuous-flow, fixed-bed column test was also performed using tertiary wastewater effluent to evaluate the PBP column's performance in more realistic applications. Tertiary wastewater effluent was collected from the fifth pass of the chlorination basin at the South Shore Water Reclamation Facility (Oak Creek, WI). Tertiary wastewater samples were analyzed for water quality parameters, as shown in the supplementary data (Table S1). The influent P_i concentration was ~0.75 mg $PO_4^{3-}L^{-1}$ and the column was operated with 0.5 mL drained PBP-NHS resin and a flow rate of 0.3 mL min^{-1}. Consecutive 1 mL samples were collected until the effluent concentration equaled the influent. A reusability test was conducted for tertiary wastewater effluent (three consecutive adsorption-desorption cycles) using these same fixed-bed column parameters, with desorption using 3 bed volumes of Tris buffer at pH 12.5.

Table 1
Continuous-flow fixed-bed column experimental design.

Parameter	Experimental Conditions		
	Influent Concentration, C_0 (mg PO_4^{3-} L^{-1})	Bed Volume, BV (mL)	Flow rate, Q (mL min^{-1})
Variable influent concentration	0.5	1.5	0.2
	1.0	1.5	0.2
	1.5	1.5	0.2
Variable bed volume	0.65	0.5	0.2
	0.65	1.0	0.2
	0.65	1.5	0.2
Variable flow rate	0.75	1.0	0.1
	0.75	1.0	0.2
	0.75	1.0	0.3

2.2.3. Statistical analysis

One-way ANOVA was performed to assess the differences in breakthrough curves for multi-cycle operation mode (reusability study), as well as to assess the differences in breakthrough curves for the selectivity study. All statistics were performed using Excel with a significance level of $\alpha = 0.05$.

2.3. Mathematical modeling of breakthrough curves

Breakthrough curves showing the ratio of effluent concentration to influent concentration with respect to time (C_t/C_0 vs t) were modeled using the empirical Adams-Bohart, Thomas, Yoon-Nelson, and Bed-Depth/Service Time (BDST) models to determine the dynamic properties of fixed-bed column operation for scaling-up purposes and performance comparison (Satya et al., 2021). These models are the most widely used to analyze adsorbent-adsorbate behavior in column-mode system operation (Patel, 2019).

2.3.1. Adams-Bohart model

The Adams-Bohart model was developed based on the surface reaction theory, which predicts that equilibrium is not immediate. Hence, the rate of adsorption is proportional to the remaining capacity of the adsorbent and the concentration of adsorbate (Chowdhury et al., 2015). The model equation and its linearized form are shown in Eq. (1) and Eq. (2), respectively.

$$\frac{C_t}{C_0} = \exp\left(K_{AB}C_0t - K_{AB}\frac{N_0Z}{U_0}\right) \quad (1)$$

$$\ln\frac{C_t}{C_0} = K_{AB}C_0t - K_{AB}\frac{N_0Z}{U_0} \quad (2)$$

where C_0 and C_t are the influent and effluent P_i concentrations (mg L^{-1}), respectively. Z is the bed height (cm), U_0 is the superficial velocity (cm min^{-1}), K_{AB} is the Adams-Bohart rate constant (L (mg-min)$^{-1}$), and N_0 is the saturation concentration (mg L^{-1}). Values for K_{AB} and N_0 are calculated from the slope and the intercept of Eq. (2), respectively.

2.3.2. Thomas model

The Thomas model was developed based on the assumption of the Langmuir adsorption isotherm with no axial dispersion, with second-order biosorption reaction kinetics (Recepoğlua et al., 2018). The Thomas model is shown in equation Eq. (3) and its linearized form is in Eq. (4).

$$\frac{C_t}{C_0} = \frac{1}{1 + \exp\left(\frac{K_{TH}q_0m}{Q} - K_{TH}C_0t\right)} \quad (3)$$

$$\ln\left(\frac{C_0}{C_t} - 1\right) = \frac{K_{TH}q_0m}{Q} - K_{TH}C_0t \quad (4)$$

where C_0 and C_t are the influent and effluent P_i concentrations (mg L^{-1}), m is the weight of PBP-resin (g), Q is the flow rate (mL min^{-1}), K_{TH} is the Thomas rate constant (L (mg-min)$^{-1}$), and q_0 is the adsorption capacity (mg g^{-1}). Values for K_{TH} and q_0 are calculated from the slope and the intercept of Eq. (4), respectively.

2.3.3. Yoon-Nelson model

The Yoon-Nelson model is a simple theoretical model derived based on the assumption that decreasing rate of adsorption for a molecule is proportional to adsorbate adsorption and breakthrough on the adsorbent (Chowdhury et al., 2013; Patel, 2019). The model equation and its linearized form are described in Eq. (5) and Eq. (6), respectively.

$$\frac{C_t}{C_0} = \frac{\exp(K_{YN}\, t - \tau K_{YN})}{1 + \exp(K_{YN}\, t - \tau K_{YN})} \tag{5}$$

$$\ln \frac{C_t}{C_0 - C_t} = K_{YN}\, t - \tau K_{YN} \tag{6}$$

where C_0 and C_t are the influent and effluent P_i concentrations (mg L^{-1}), K_{YN} is Yoon-Nelson rate constant (min^{-1}), and τ is the time required for 50% adsorbate breakthrough (min). Values for K_{YN} and τ can be found from the slope and the intercept of Eq. (6), respectively.

2.3.4. Bed-Depth/Service Time model

The BDST model is used to predict how long the column's packed-bed material can last before regeneration or replacement (Samarghandi et al., 2014). The BDST model was developed based on a surface chemical reaction between the adsorbate and the unused capacity of the adsorbent, with negligible intraparticle diffusion (Oh et al., 2009; Samarghandi et al., 2014). The linear relationship of bed depth (i.e., height) to service time is given by Eq. (7) (Oh et al., 2009).

$$t = \frac{N_0 Z}{C_0 F} - \frac{1}{K_{BDST} C_0} \ln\left(\frac{C_0}{C_t} - 1\right) \tag{7}$$

where C_0 and C_t are the influent and effluent P_i concentrations (mg L^{-1}), K_{BDST} is the rate constant of the BDST model (L (mg-min)$^{-1}$), N_0 is the adsorption capacity (mg L^{-1}), Z is the bed depth (cm), F is the linear velocity (cm min^{-1}), and t is the service time (min).

3. Results and discussion

3.1. Fixed-bed adsorption studies

To design and run fixed-bed columns for realistic full-scale operation, smaller-scale breakthrough curves tested as a function of operating parameters are needed (Manjunath and Kumar, 2021). To inform scale-up and implementation, the breakthrough curves from the continuous-flow, fixed-bed column experiments using PBP-NHS are discussed in the following sections.

3.1.1. Column operating parameters

3.1.1.1. Effect of influent P_i concentration. The effect of influent P_i concentration on the breakthrough curve was investigated for influent levels of 0.5, 1.0, and 1.5 mg $PO_4^{3-}L^{-1}$, as illustrated in Fig. 1a. Increasing influent P_i concentration resulted in a steeper breakthrough curve due to faster mass transfer. Time to breakthrough was faster as influent P_i concentration increased, with values of 100, 55, and 45 min for 0.5, 1.0, and 1.5 mg $PO_4^{3-}L^{-1}$, respectively (145, 100, and 60 min for exhaustion). At the lowest influent P_i concentration tested (0.5 mg $PO_4^{3-}L^{-1}$) the number of treated bed volumes was 20, or approximately twice that treated when the P_i concentration doubled. This general trend (i.e., increasing the concentration expedites breakthrough) was expected because the available active PBP binding sites were more rapidly occupied in the presence of higher P_i concentration, and the column was saturated more quickly. Yet, the exact timing of column breakthrough and exhaustion under variable conditions is needed for scale-up and must be determined experimentally.

3.1.1.2. Effect of bed volume. The effect of bed volume (controlled by bed height) on the breakthrough curve is shown in Fig. 1b. Noticeably longer time to breakthrough was obtained as the bed volume increased

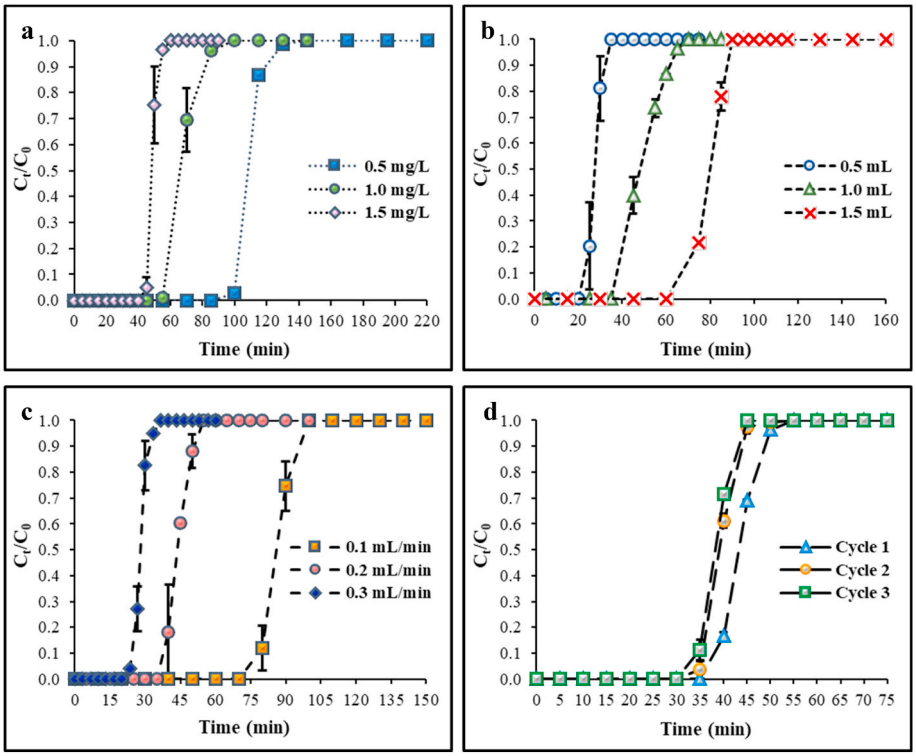

Fig. 1. Breakthrough curves (ratio of effluent to influent P_i concentration [C_t/C_0] as a function of operating time) under different column operating parameters: (a) influent P_i concentration, (b) bed volume, (c) flow rate, and (d) multi-cycle column experiment at an influent concentration of 1.1 mg L^{-1}, bed volume of 1 mL, and flow rate of 0.2 mL min^{-1}. Note that the maximum time varies among the panels. All column tests were conducted in duplicate, as indicated by the error bars.

from 0.5 mL to 1.5 mL. Time to breakthrough was 25, 45, and 75 min for 0.5, 1.0, and 1.5 mL of drained PBP-NHS resin, respectively (35, 70, and 90 min for exhaustion). Increasing the bed volume provided more PBP active binding sites in the column to capture P_i; therefore, a longer time was needed to reach complete saturation (column exhaustion). The number of treated bed volumes doubled from 5 to approximately 10 as bed volume doubled, which suggests a uniform distribution of PBP adsorption on NHS-activated Sepharose. This lab-scale breakthrough data can be used to advance scaled-up design for large-scale column applications.

3.1.1.3. Effect of feed flow rate. The effect of influent P_i flow rate on the breakthrough curve is shown in Fig. 1c. As expected, time to breakthrough was more rapid as influent P_i flow rate increased. Time to breakthrough was 80, 40, and 23 min for 0.1, 0.2, and 0.3 mL min^{-1}, respectively (100, 55, and 37 min for exhaustion). The available PBP binding sites were rapidly occupied when higher rates of P_i molecules entered the column.

3.1.1.4. Reusability. To evaluate the system's reusability, consecutive adsorption-desorption cycles were conducted three times, as shown in Fig. 1d. The desorption cycle, which consisted of three bed volumes of wash with pH 12.5 Tris buffer, released all P_i from the column. For the first cycle, the breakthrough time was 40 min, and the exhaustion time was 55 min with a treated bed volume of 8 mL. For the second cycle, the breakthrough time was 40 min, and the exhaustion time was 50 min with a treated bed volume of 8 mL. For the third cycle, the breakthrough time was 35 min, and the exhaustion time was 45 min with a treated bed volume of 7 mL. The experimental data showed slight variation in the breakthrough curves between the cycles. However, one-way ANOVA showed no significant difference between the three cycles ($p = 0.93$). Thus, there was no loss in PBP-NHS resin performance for at least three cycles of adsorption/desorption in column mode operation. Venkiteshwaran et al. (2018) similarly showed no loss in performance over 10 cycles of adsorption/desorption in batch-mode operation.

3.1.2. Selectivity of PBP-NHS resin in more complex matrices

3.1.2.1. Phosphate-only versus multi-ion buffer. An adsorbent's selectivity is important for actual applications in which many potential competitors may be present in solution. Higher selectivity offers higher removal in the presence of other constituents, and also leads to a purer recovered product, which enhances the value of the process. The selectivity of PBP-NHS resin was investigated in parallel sets of experiments using P_i-only solution and multi-ion synthetic solution (Fig. 2a). There was no significant difference between the breakthrough curves ($p = 0.81$), with each having a breakthrough time of 20 min with 4 mL treated bed volume and time to exhaustion of approximately 35 min. This demonstrates the high P_i-selectivity of PBP-NHS resin, in agreement with previous batch tests (Venkiteshwaran et al., 2020).

For comparison, Fig. 2b illustrates the breakthrough curves for P_i-only solution and multi-ion solution experiments using commercially available, phosphate-selective ion exchange resin, LayneRT™. Noticeably, LayneRT™ resin's performance was affected by competing anions, where competing anions decreased the time to exhaustion by 20 min. Additionally, the LayneRT™ resin's P_i removal capacity (40 mg P g^{-1} LayneRT resin) dropped by 20% due to the presence of competing anions. Accordingly, although LayneRT™ resin offers much more selective P_i adsorption relative to common adsorbents such as granular activated carbon, competition due to other ions can impact performance, as also reported in other studies (Martin et al., 2018; Ownby et al., 2021; Tang, 2015; Williams et al., 2015; You et al., 2016). Conversely, the presence of other anions and cations did not impede P_i adsorption using the PBP-NHS resin.

3.1.2.2. Wastewater. To investigate PBP-NHS resin's performance under more realistic conditions, tertiary wastewater effluent was tested in continuous-flow, fixed-bed columns. The breakthrough curves for a single-column run and multi-cycle column run are illustrated in Fig. 3a and Fig. 3b, respectively. Compared to the P_i synthetic solution experiments, the wastewater breakthrough curve had a typical S-shape with a breakthrough time of 20 min and exhaustion time of 43 min. The curve was more gradual (i.e., there was not a quick jump in the effluent concentration), with 23 min between breakthrough and exhaustion compared to 10 min using the P_i-only solution. The tertiary wastewater components likely served as a physical barrier, i.e., causing steric hindrance to prevent P_i from accessing the immobilized PBP's active binding, thus extending the time to exhaustion. While extending the time to exhaustion can be beneficial in application, it would be important to monitor effluent concentrations to ensure compliance with the discharge limits during the extended cycle. Although the shape of the breakthrough curves differed, there was no difference in adsorption capacity as the PBP-NHS resin achieved 96% of its maximum theoretical capacity in both synthetic solution and wastewater (20 μg P g^{-1} PBP-NHS resin).

Three consecutive cycles of adsorption/desorption using the column to treat wastewater showed no significant reduction ($p = 0.91$) in the time to exhaustion and the treated bed volume. The first cycle had a breakthrough time of 23 min and exhaustion time of 40 min with a 7-mL treated bed volume. The second and third cycles had breakthrough times of 20 min and exhaustion times of 37 min with a 6-mL treated bed volume.

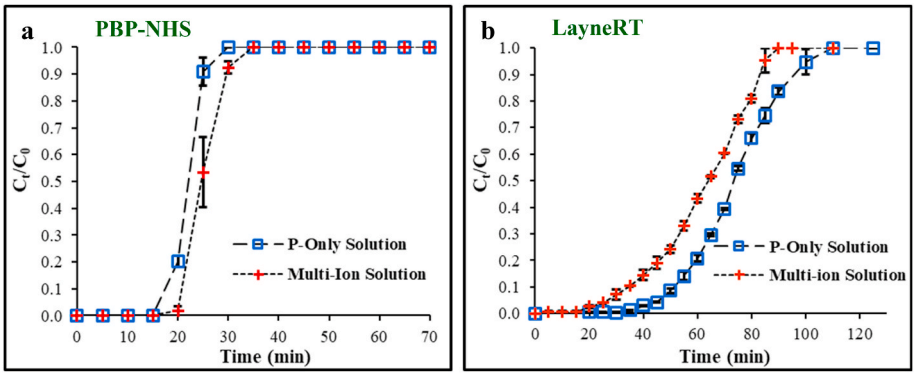

Fig. 2. Comparison of breakthrough curves (ratio of effluent to influent P_i concentration [C_t/C_0] as a function of operating time) using P_i-only solution versus multi-ion solution (containing phosphate, sulfate, chloride, nitrate, and bicarbonate ions) for two different phosphate-selective resins: (a) PBP-NHS resin, and (b) LayneRT™ resin. All column tests were conducted in duplicate, as indicated by the error bars.

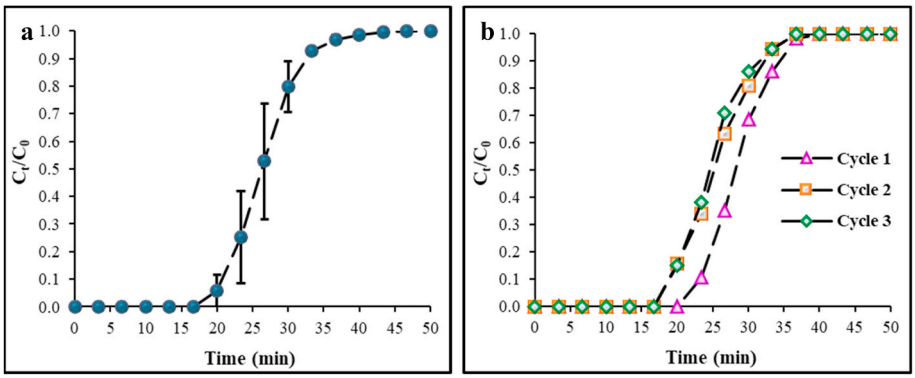

Fig. 3. Breakthrough curves (ratio of effluent to influent P_i concentration [C_t/C_0] as a function of operating time) for tertiary wastewater effluent tests: (a) single-column experiment and (b) multi-cycle column experiment. Both tests were performed using a bed volume of 0.5 mL, flow rate of 0.3 mL min^{-1}, and influent phosphate concentration of 0.75 mg $PO_4^{3-}L^{-1}$. All column tests were conducted in duplicate, as indicated by the error bars.

3.2. Mathematical modeling of breakthrough curves

3.2.1. Breakthrough curve fitting with the Adams-Bohart, Thomas, and Yoon-Nelson models

Parameters for the Adams-Bohart, Thomas, and Yoon Nelson models are provided in Table 2. A comparison between the empirical and theoretical breakthrough curves predicted using these models at different influent P_i concentrations is shown in the Supplementary Data (Figs. S2-S4). The linear regression analyses and the breakthrough curve comparison at different bed volumes and flow rates for all models are shown in the Supplementary Data (Figs. S5-S10). The breakthrough curves were well fit using the Thomas and Yoon-Nelson models ($R^2 > 0.95$). The strong alignment of the experimental data with the Thomas model suggests that P_i adsorption occurs in a monolayer (Langmuir isotherm assumption) with no axial dispersion. In contrast, the Adams-Bohart model only fit well to the initial part of the breakthrough curve ($C_t/C_0 < 0.1$). This agrees with previous reports that the Adams-Bohart model is usually used to describe only the initial part of the breakthrough curve (Singh et al., 2020).

As influent P_i concentration increased, the Thomas model rate constant (K_{TH}) decreased, while the sorption capacity (q_0) increased. The same trend was observed for the Adams-Bohart model. Higher adsorbate concentration increases the resistance to mass transfer and thus decreases the rate constants (Manjunath and Kumar, 2021). Conversely, the Yoon-Nelson rate constant (K_{YN}) increased as influent P_i concentration increased. Using the Yoon-Nelson model, the time to C_t/C_0 = 50% (τ) decreased from 96.7 min to 44.2 min as P_i concentration increased from 0.5 to 1.5 mg $PO_4^{3-}L^{-1}$.

The percent error (ε) between τ determined using the experimental data versus the predicted model was 8%–12%. For the Thomas model, the error between C_t/C_0 = 50% values determined using the experimental data versus the predicted model was 3%–9%, suggesting that both Thomas and Yoon-Nelson models provide good predictions of the dynamic behavior of the PBP-NHS resin column.

All model rate constants decreased as bed volume increased, while the sorption capacity increased. Greater bed depth slows the mass transfer rate by increasing the residence time between the adsorbate and adsorbent (Manjunath and Kumar, 2021). The time required for C_t/C_0 = 50% (τ) increased from 22.4 min to 67.6 min as bed volume increased from 0.5 to 1.5 mL of drained PBP-NHS resin. The error between experimental and predicted C_t/C_0 = 50% values was 16%–20% using the Yoon-Nelson model and 0.1%–0.4% using the Thomas model.

The Thomas model rate constant (K_{TH}) and sorption capacity (q_0) increased as flow rate increased. The same trend was observed for the Adams-Bohart model, where the mass transfer coefficient (K_{AB}) and saturation concentration (N_0) increased as influent P_i flow rate increased. Similarly, the Yoon-Nelson rate constant (K_{YN}) increased as influent P_i flow rate increased. The time required for C_t/C_0 = 50% (τ) decreased from 76.5 min to 24.8 min as influent P_i flow rates increased from 0.1 to 0.3 mL. The error (ε) between experimental and predicted values was 11% for all operating flow rates using the Yoon-Nelson model and 0.3%–0.7% using the Thomas model.

3.2.2. Application of the Bed-Depth/Service Time (BDST) model

Service time reflects the useful operating time prior to regeneration or replacing the column media under specific operating conditions and is useful to scale up and optimize a fixed-bed adsorption system (Ang et al., 2020). The predicted bed service time at different influent P_i concentrations and flow rates using the BDST model is illustrated in Fig. 4, with 10% and 90% breakthrough. Experimental data fit to the

Table 2
Adams-Bohart, Thomas, and Yoon-Nelson model parameters for varying column operating conditions.

				Adams-Bohart model			Thomas model			Yoon-Nelson model		
C_0 (mg L^{-1})	Z (cm)	Q (mL min^{-1})	EBCT (min)	K_{AB} (L [mg-min]$^{-1}$)	N_0 (mg L^{-1})	R^2	K_{TH} (L [mg-min]$^{-1}$)	q_0 (mg g^{-1})	R^2	K_{YN} (min^{-1})	T (min)	R^2
0.5	3	0.2	7.5	0.209	9.51	0.78	0.458	12.1	0.95	0.260	96.7	0.95
1.0	3	0.2	7.5	0.164	10.5	0.80	0.276	13.1	0.95	0.308	57.5	0.89
1.5	3	0.2	7.5	0.203	10.5	0.81	0.429	13.8	0.97	0.630	44.2	0.97
0.65	1	0.2	2.5	0.249	8.62	0.85	0.882	10.0	1.00	0.562	22.4	1.00
0.65	2	0.2	5.0	0.055	9.01	0.90	0.266	9.32	0.97	0.137	38.2	0.96
0.65	3	0.2	7.5	0.156	8.03	0.97	0.376	10.3	1.00	0.169	67.6	1.00
0.75	2	0.1	10.0	0.139	7.45	0.85	0.404	9.43	1.00	0.308	76.5	1.00
0.75	2	0.2	5.0	0.143	8.07	0.83	0.458	9.63	1.00	0.350	39.1	1.00
0.75	2	0.3	3.3	0.433	7.00	0.88	0.857	8.78	0.99	0.625	24.8	0.99

C_0, influent P_i concentration (mg PO_4^{3-} L^{-1}); Z, bed depth (cm); Q, flow rate (mL min^{-1}); EBCT, empty bed contact time (min); K_{AB}, mass transfer coefficient (L [mg-min]$^{-1}$); N_0, saturation concentration (mg L^{-1}); K_{TH}, Thomas model rate constant (L [mg-min]$^{-1}$); q_0, sorption capacity (mg g^{-1}); K_{YN}, Yoon-Nelson rate constant (min^{-1}); τ, time required for 50% breakthrough (min).

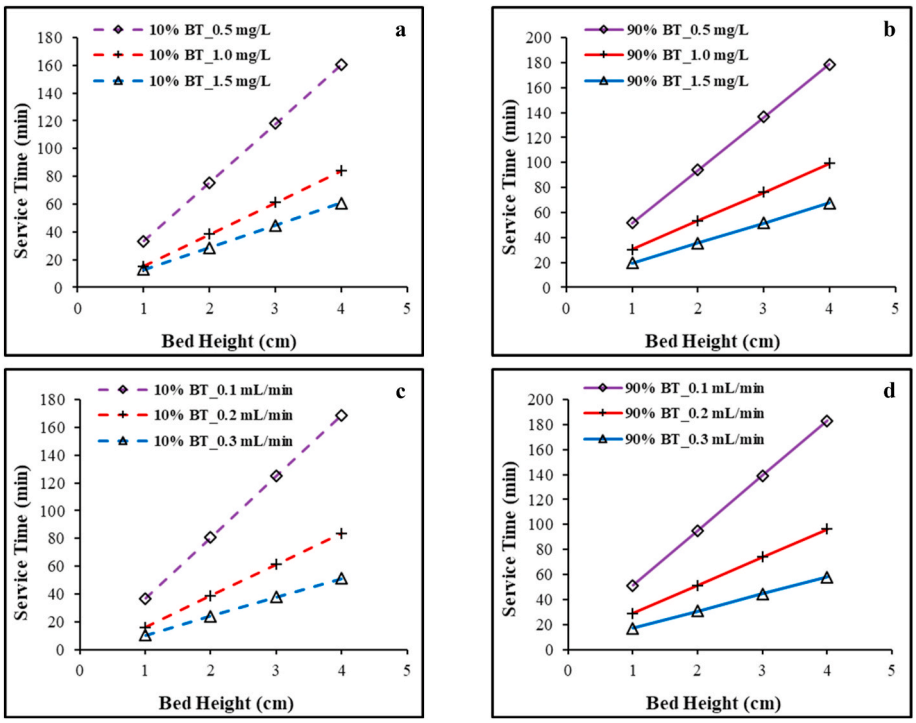

Fig. 4. Calculated bed service time for breakthrough (10% BT; panels a and c) and exhaustion (90% BT; panels b and d). Panels a and b illustrate the impact of different influent phosphate concentrations, while panels c and d illustrate the impact of different flow rates.

BDST equation ($R^2 > 0.95$) are shown in the Supplementary Data (Figs. S11 and S12). For the tertiary wastewater effluent (Fig. S13, Fig. S14, and Table S2), the models also performed well ($R^2 = 0.99$, error 1%).

Results from the lab-scale column breakthrough tests can be used to design large-scale columns using the scale-up approach (Jung et al., 2017). An example of the scale-up design calculations and parameters is provided in the Supplementary Data (Table S3).

4. Conclusions

A comprehensive lab-scale, fixed-bed column study of P_i adsorption using PBP-NHS resin was conducted in this study. Highly selective P_i separation was observed, as illustrated by the sharp S-shape of the breakthrough curves. There was no significant decline in the column's performance over three consecutive cycles in either synthetic solution or tertiary wastewater, substantiating PBP-NHS resin's reusability, as well as the potential to recover the captured P_i for subsequent reuse. Furthermore, the resin's capacity was unaffected by competing anions, whereas the LayneRT™ column capacity dropped 20% in the presence of other anions. The Thomas and Yoon-Nelson models satisfactorily described the breakthrough characteristics for PBP-NHS resin and BDST analysis predicted breakthrough service times. This study supports the potential for implementation of fixed-bed, flow through systems featuring the high-affinity PBP bioadsorbent to effectively remove P_i to ultra-low levels while recovering P_i from wastewater. The results herein inform design and scale up of PBP-NHS adsorption systems, although setting-specific parameters must also be accounted for during system design and implementation.

Credit author statement

Faten Hussein: Conceptualization, Methodology, Validation, Formal analysis, Investigation, Writing – original draft, Writing – review & editing, Visualization. Brooke K Mayer: Conceptualization, Resources, Writing – review & editing, Supervision, Project administration, Funding acquisition.

Declaration of competing interest

The authors declare the following financial interests/personal relationships which may be considered as potential competing interests: B. Mayer is a co-inventor on a patent application entitled "Process for controlled adsorption and desorption of phosphate from liquids using phosphate-selective proteins". The authors declare no other competing interests.

Acknowledgment

This work was supported by CAREER award 1554511 from the National Science Foundation (NSF). All opinions expressed in this paper are the authors' and do not reflect the views of NSF. We thank Synthia Parveen Mallick and Donald Ryan from the Water Quality Center at Marquette University for their help in measuring sulfate and dissolved organic carbon characteristics of the tertiary wastewater effluent.

Appendix A. Supplementary data

Supplementary data to this article can be found online at https://doi.org/10.1016/j.chemosphere.2022.133908.

Supplementary Data

Supplementary data for this article can be found online.

References

Ang, T.N., Young, B.R., Taylor, M., Burrell, R., Aroua, M.K., Baroutian, S., 2020. Breakthrough analysis of continuous fixed-bed adsorption of sevoflurane using activated carbons. Chemosphere 239, 124839. https://doi.org/10.1016/j.chemosphere.2019.124839.

APHA, 2005. Standard Methods for the Examination of Water and Wastewater, twenty-first ed. American Public Health Association, Washington, D.C.

Bui, T.H., Hong, S.P., Yoon, J., 2018. Development of nanoscale zirconium molybdate embedded anion exchange resin for selective removal of phosphate. Water Res. 134, 22–31. https://doi.org/10.1016/J.WATRES.2018.01.061.

Choi, S.S., Lee, H.M., Ha, J.H., Kang, D.G., Kim, C.S., Seo, J.H., Cha, H.J., 2013. Biological removal of phosphate at low concentrations using recombinant Escherichia coli expressing phosphate-binding protein in periplasmic space. Appl. Biochem. Biotechnol. 171, 1170–1177. https://doi.org/10.1007/s12010-013-0187-1.

Chowdhury, Z.Z., Hamid, S.B.A., Zain, S.M., 2015. Evaluating design parameters for breakthrough curve analysis and kinetics of fixed bed columns for Cu(II) cations using Lignocellulosic wastes zaira. Bioresources 10, 732–749.

Chowdhury, Z.Z., Zain, S.M., Rashid, A.K., Rafique, R.F., Khalid, K., 2013. Breakthrough curve analysis for column dynamics sorption of Mn(II) ions from wastewater by using Mangostana garcinia peel-based granular-activated carbon. J. Chem. 2013, 1–8. https://doi.org/10.1155/2013/959761.

Hu, A., Ren, G., Che, J., Guo, Y., Ye, J., Zhou, S., 2020. Phosphate recovery with granular acid-activated neutralized red mud: fixed-bed column performance and breakthrough curve modelling. J. Environ. Sci. (China) 90, 78–86. https://doi.org/10.1016/j.jes.2019.10.018.

Huang, H., Zhang, D.D., Li, J., Guo, G., Tang, S., 2017. Phosphate recovery from swine wastewater using plant ash in chemical crystallization. J. Clean. Prod. 168, 338–345. https://doi.org/10.1016/J.JCLEPRO.2017.09.042.

Hussein, F.B., Venkiteshwaran, K., Mayer, B.K., 2020. Cell surface-expression of the phosphate-binding protein PstS: system development, characterization, and evaluation for phosphorus removal and recovery. J. Environ. Sci. (China) 92, 129–140. https://doi.org/10.1016/j.jes.2020.02.016.

Jia, Z., Zeng, W., Xu, H., Li, S., Peng, Y., 2020. Adsorption removal and reuse of phosphate from wastewater using a novel adsorbent of lanthanum-modified platanus biochar. Process Saf. Environ. Protect. 140, 221–232. https://doi.org/10.1016/j.psep.2020.05.017.

Jung, K.W., Jeong, T.U., Choi, J.W., Ahn, K.H., Lee, S.H., 2017. Adsorption of phosphate from aqueous solution using electrochemically modified biochar calcium-alginate beads: batch and fixed-bed column performance. Bioresour. Technol. 244, 23–32. https://doi.org/10.1016/j.biortech.2017.07.133.

Kuroda, A., Kunimoto, H., Morohoshi, T., Ikeda, T., Kato, J., Takiguchi, N., Miya, A., Ohtake, H., 2000. Evaluation of phosphate removal from water by immobilized phosphate-binding protein PstS. J. Biosci. Bioeng. 90, 688–690. https://doi.org/10.1016/S1389-1723(00)90020-3.

Ledvina, P.S., Tsai, A.L., Wang, Z., Koehl, E., Quiocho, F.A., 1998. Dominant role of local dipolar interactions in phosphate binding to a receptor cleft with an electronegative charge surface: equilibrium, kinetic, and crystallographic studies. Protein Sci. 7, 2550–2559. https://doi.org/10.1002/pro.5560071208.

Li, Q., Yu, Z., Shao, X., He, J., Li, L., 2009. Improved phosphate biosorption by bacterial surface display of phosphate-binding protein utilizing ice nucleation protein. FEMS Microbiol. Lett. 299, 44–52. https://doi.org/10.1111/j.1574-6968.2009.01724.x.

Luecke, H., Quiocho, F., 1990. High specificity of a phosphate transport protein determined by hydrogen bonds. Lett. To Nat 347, 402–406. https://doi.org/10.1038/346183a0.

Manjunath, S.V., Kumar, M., 2021. Simultaneous removal of antibiotic and nutrients via Prosopis juliflora activated carbon column: performance evaluation, effect of operational parameters and breakthrough modeling. Chemosphere 262. https://doi.org/10.1016/j.chemosphere.2020.127820.

Martin, B.D., De Kock, L., Gallot, M., Guery, E., Stanowski, S., MacAdam, J., McAdam, E. J., Parsons, S.A., Jefferson, B., 2018. Quantifying the performance of a hybrid anion exchanger/adsorbent for phosphorus removal using mass spectrometry coupled with batch kinetic trials. Environ. Technol. 39, 2304–2314. https://doi.org/10.1080/09593330.2017.1354076.

Mayer, B.K., Gerrity, D., Rittmann, B.E., Reisinger, D., Brandt-Williams, S., 2013. Innovative strategies to achieve low total phosphorus concentrations in high water flows. Crit. Rev. Environ. Sci. Technol. 43, 409–441. https://doi.org/10.1080/10643389.2011.604262.

Oh, H.-J., Choung, Y.-K., Lee, S., Choi, J.-S., Hwang, T.-M., Kim, J.H., 2009. Adsorption of methylene blue by phoenix tree leaf powder in a fixed-bed column: experiments and prediction of breakthrough curves. Desalination 238, 333–346. https://doi.org/10.1016/j.desal.200.

Ownby, M., Desrosiers, D.A., Vaneeckhaute, C., 2021. Phosphorus removal and recovery from wastewater via hybrid ion exchange nanotechnology: a study on sustainable regeneration chemistries. npj Clean Water 4, 1–8. https://doi.org/10.1038/s41545-020-00097-9.

Pap, S., Kirk, C., Bremner, B., Turk Sekulic, M., Shearer, L., Gibb, S.W., Taggart, M.A., 2020. Low-cost chitosan-calcite adsorbent development for potential phosphate removal and recovery from wastewater effluent. Water Res. 173, 115573. https://doi.org/10.1016/j.watres.2020.115573.

Patel, H., 2019. Fixed-bed column adsorption study; a comprehensive review. Appl. Water Sci. 9, 1–17. https://doi.org/10.1007/s13201-019-0927-7.

Qiu, H., Liang, C., Yu, J., Zhang, Q., Song, M., Chen, F., 2017. Preferable phosphate sequestration by nano-La(III) (hydr)oxides modified wheat straw with excellent properties in regeneration. Chem. Eng. J. 315, 345–354. https://doi.org/10.1016/J.CEJ.2017.01.043.

Recepoğlua, Y.K., Kabay, N., Ipek, I.Y., Arda, M., Yüksel, M., Yoshizuka, K., Nishihama, S., 2018. Packed bed column dynamic study for boron removal from geothermal brine by a chelating fiber and breakthrough curve analysis by using mathematical models. Desalination 437, 1–6. https://doi.org/10.1016/j.desal.2018.02.022.

Samarghandi, M.R., Hadi, M., McKay, G., 2014. Breakthrough curve analysis for fixed-bed adsorption of azo dyes using novel pine cone-derived active carbon. Adsorpt. Sci. Technol. 32, 791–806. https://doi.org/10.1260/0263-6174.32.10.791.

Satya, A., Harimawan, A., Sri Haryani, G., Johir, M.A.H., Nguyen, L.N., Nghiem, L.D., Vigneswaran, S., Ngo, H.H., Setiadi, T., 2021. Fixed-bed adsorption performance and empirical modelingof cadmium removal using adsorbent prepared from the cyanobacterium Aphanothece sp cultivar. Environ. Technol. Innovat. 21, 101194. https://doi.org/10.1016/j.eti.2020.101194.

Singh, S., Chandra Srivastava, V., Goyal, A., Deo Mall, I., 2020. Breakthrough modeling of furfural sorption behavior in a bagasse fly ash packed bed. Environ. Eng. Res. 25, 104–113. https://doi.org/10.4491/eer.2018.407.

Solscheid, C., Kunzelmann, S., Davis, C.T., Hunter, J.L., Nofer, A., Webb, M.R., 2015. Development of a reagentless biosensor for inorganic phosphate, applicable over a wide concentration range. Biochemistry 54, 5054–5062. https://doi.org/10.1021/acs.biochem.5b00449.

Tang, Y., 2015. Parameters Affecting Phosphate Sorption from Sludge Liquors by Hybrid Anion Sorbents. the Karlsruhe Institute of Technology.

Venkiteshwaran, K., Pokhrel, N., Hussein, F., Antony, E., Mayer, B.K., 2018. Phosphate removal and recovery using immobilized phosphate binding proteins. Water Res. X 1, 1–9. https://doi.org/10.1016/j.wroa.2018.09.003.

Venkiteshwaran, K., Wells, E., Mayer, B.K., 2021. Immobilized phosphate-binding protein can effectively discriminate against arsenate during phosphate adsorption and recovery. Water Environ. Res. 93, 1173–1178. https://doi.org/10.1002/wer.1498.

Venkiteshwaran, K., Wells, E., Mayer, B.K., 2020. Kinetics, affinity, thermodynamics, and selectivity of phosphate removal using immobilized phosphate-binding proteins. Environ. Sci. Technol. 54, 10885–10894. https://doi.org/10.1021/acs.est.0c02272.

Williams, A.T., Zitomer, D.H., Mayer, B.K., 2015. Ion exchange-precipitation for nutrient recovery from dilute wastewater. Environ. Sci. Water Res. Technol. 1, 832–838. https://doi.org/10.1039/c5ew00142k.

Xu, Q., Chen, Z., Wu, Z., Xu, F., Yang, D., He, Q., Li, G., Chen, Y., 2019. Novel lanthanum doped biochars derived from lignocellulosic wastes for efficient phosphate removal and regeneration. Bioresour. Technol. 289, 121600. https://doi.org/10.1016/J.BIORTECH.2019.121600.

Yang, S., Jin, P., Wang, X., Zhang, Q., Chen, X., 2016. Phosphate recovery through adsorption assisted precipitation using novel precipitation material developed from building waste: behavior and mechanism. Chem. Eng. J. 292, 246–254. https://doi.org/10.1016/j.cej.2016.02.006.

Yang, Y., Ballent, W., Mayer, B.K., 2016. High-affinity phosphate-binding protein (PBP) for phosphorous recovery: proof of concept using recombinant Escherichia coli. FEMS Microbiol. Lett. 363, 1–6. https://doi.org/10.1093/femsle/fnw240.

Yanyan, L., Kurniawan, T.A., Zhu, M., Ouyang, T., Avtar, R., Dzarfan Othman, M.H., Mohammad, B.T., Albadarin, A.B., 2018. Removal of acetaminophen from synthetic wastewater in a fixed-bed column adsorption using low-cost coconut shell waste pretreated with NaOH, HNO3, ozone, and/or chitosan. J. Environ. Manag. 226, 365–376. https://doi.org/10.1016/J.JENVMAN.2018.08.032.

You, X., Farran, A., Guaya, D., Valderrama, C., Soldatov, V., Cortina, J.L., 2016. Phosphate removal from aqueous solutions using a hybrid fibrous exchanger containing hydrated ferric oxide nanoparticles. J. Environ. Chem. Eng. 4, 388–397. https://doi.org/10.1016/j.jece.2015.11.032.